Science of the Total Environment 955 (2024) 177227

Contents lists available at ScienceDirect

Science of the Total Environment

journal homepage: www.elsevier.com/locate/scitotenv

Phosphorus removal from municipal wastewater using calcium/iron oxide composites: Adsorption efficiency and impact on plant growth

Jūlija Karasa [a], Rūta Ozola-Davidāne [a,b,*], Kamila Gruškeviča [c], Katrīna Anna Ozoliņa [a], Līga Irbe Mikosa [c], Juris Kostjukovs [a]

[a] University of Latvia, Faculty of Science and Technology, Department of Environmental Protection, Jelgavas Street 1, Riga, LV-1004, Latvia
[b] Latvia University of Life Sciences and Technologies, Faculty of Forest and Environmental Sciences, Akademijas Street 11, Jelgava, LV-3001, Latvia
[c] Riga Technical University, Water Systems and Biotechnology Institute, Kipsalas 6a-263, Riga, LV-1048, Latvia

HIGHLIGHTS

- Ca/FeOxides derived from natural pigments can reclaim P from wastewater.
- Ca/FeOxide T showed a maximum P adsorption capacity of 83.33 mg/g.
- P-loaded CaFeOxides and Polonite® enhanced *T. aestivum* seedling growth.

GRAPHICAL ABSTRACT

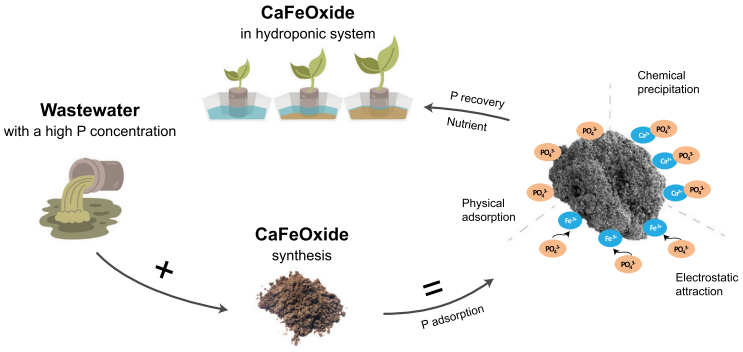

ARTICLE INFO

Guest Editor: Giorgio Mannina

Keywords:
Iron oxide pigments
Phosphorus recovery
Srebrodolskite
Soil amendment
Wastewater

ABSTRACT

Phosphate minerals are crucial for the production of fertilizers, but limited availability does not meet the growing agricultural demand. At the same time, the discharge of phosphorus by municipal wastewater treatment plants leads to eutrophication. Removal and recovery of phosphorus from wastewater can both provide nutrients to agriculture and decrease eutrophication. This research aims to evaluate phosphorus removal from municipal wastewater in Latvia by mineral-based calcium/iron composites and examine spent oxides' phytotoxic effect on plant growth. Two CaFeOxides from Latvian earth pigments (iron oxide pigments) deposits were synthesized and characterised by X-ray powder diffraction, differential scanning calorimetry/thermogravimetry, scanning electron microscopy-energy dispersive X-ray analysis and specific surface area analysis. Adsorption properties of obtained oxides were evaluated with a standard phosphate solution, and real municipal wastewater. The phytotoxic effect of P-loaded composites was evaluated in a hydroponic system with common wheat (*Triticum aestivum*). The results indicated that calcium/iron oxide composites have higher P adsorption efficiency than the commercial Polonite material. The maximum sorption capacity of CaFeOxides was 63.29 and 83.33 mg P/g, and 53.19 mg/g for Polonite. Furthermore, the P-loaded CaFeOxides demonstrated no phytotoxic effect on the

* Corresponding author at: Latvia University of Life Sciences and Technologies, Faculty of Forest and Environmental Sciences, Akademijas Street 11, Jelgava LV-3001, Latvia.
E-mail address: ruta.ozola-davidane@lbtu.lv (R. Ozola-Davidāne).

https://doi.org/10.1016/j.scitotenv.2024.177227
Received 4 August 2024; Received in revised form 3 October 2024; Accepted 24 October 2024
Available online 31 October 2024

growth of *Triticum aestivum*, and at higher CaFeOxides concentrations, morphological and physiological parameters of wheat increased, showing great potential for reuse in agriculture.

1. Introduction

Phosphorus (P), sourced primarily from phosphate rock deposits, is a crucial and irreplaceable element used for global food production and various other industries (Spears et al., 2022). However, its unequal distribution among countries (Morocco alone occupies 75 % of the world's P reserves) poses geopolitical and economic risks in terms of resource distribution and pricing (Li et al., 2023a). Yet, improper utilization leads to environmental pollution, primarily from agricultural runoff, industrial and municipal wastewater, contributing to eutrophication and reducing surface water quality (Salimova et al., 2020).

Various methods exist for P removal including adsorption/ion exchange, chemical precipitation/coagulation, membrane separation, constructed wetlands, reverse osmosis, electrodialysis, each with distinct advantages and challenges (Saaremäe et al., 2014; Wang et al., 2021; Szota et al., 2024; Ping et al., 2024). The coagulation/precipitation method, for instance, utilizes a range of sorbents either alongside or instead of traditional coagulants to achieve effective P removal. These include calcinated materials (Park et al., 2022), mesoporous silica (Huang et al., 2015; Jing et al., 2020), biochars derived from natural materials (Antunes et al., 2018; Almanassra et al., 2021), sewage sludge biochar (Yin et al., 2019), and other biowaste-derived materials (Bellahsen et al., 2021; Feng et al., 2022). Additionally, hydrogels (Othman et al., 2018), magnetic adsorbents (Bacelo et al., 2020), vivianite (Wang et al., 2023), calcium-modified powdered activated carbon with chitosan (Li et al., 2023b), hydroxyapatite (Li et al., 2022; Ferraro et al., 2023), clay and clay minerals (Jemeljanova et al., 2019) and zeolites (Alshameri et al., 2014; He et al., 2016).

Studies have examined calcium/iron-rich adsorbents for P removal, including Fe oxide-doped halloysite nanotubes (Almasri et al., 2019), Ca/Fe composites (Wu et al., 2021), Ca-rich sepiolite (Deng et al., 2021), and Ca/Fe-rich biochar (Yu et al., 2022). Ca/Fe-rich adsorbents can also originate from industrial wastes and by-products like bauxite residues (Barca et al., 2022) or red mud (Park et al., 2021), steel-making slag (Vu et al., 2023; Chen, 2021) as well as natural sources like Brownmillerite minerals (Gupta et al., 2015; Bedon et al., 2021). Latvia has several earth pigment deposits historically used for natural pigment manufacturing, including ochre and burnt ochre (umber) (Kokins et al., 2018). Previous work reported that heat treatment of Latvian earth pigments formed calcium iron oxide composites, mainly the Brownmillerite subgroup mineral Srebrodolskite ($Ca_2Fe_2O_5$), which can be used as effective P adsorbents (Karasa et al., 2023). Recently, it was discovered that Srebrodolskite can be used as a rapid water disinfectant (Vanags et al., 2021).

Despite various studies examining P binding with adsorbents, only a limited number of investigations have tested the proposed adsorbents with actual wastewater (Cucarella et al., 2009; Liu et al., 2015; Feng et al., 2022) or polluted surface waters (Lee et al., 2021). Even fewer studies have demonstrated the recycling of spent sorbents (Faraji et al., 2020) or their reuse as fertilizers (Cucarella et al., 2009; Liu et al., 2015). While sorbents are rarely studied from a recycling perspective, struvite (magnesium ammonium phosphate) has become a widely used alternative method in wastewater treatment in recent years, due to its ability to efficiently recover nutrients and serve as a bioavailable, slow-release fertilizer (Li et al., 2019; Battaz et al., 2024).

This research aims to evaluate phosphorus removal from municipal wastewater by Latvian mineral-based calcium/iron oxides and examine spent oxides' phytotoxic effect on plant growth. Data from CaFeOxide sorbents were compared to commercially available adsorbent Polonite® (Ecofiltration sp. z o.o, Poland). This study is novel as no studies have explored Srebrodolskite's minerals properties for water treatment, P removal, or its potential reuse as a soil amendment in agriculture.

2. Materials and methods

2.1. Raw materials

Natural origin iron oxide containing pigments - earth colours - were used to synthesise calcium/iron composites for P removal from wastewater. Raw materials for the composites of this research come from two local deposits in Latvia: Talicka (Madonas district 56 °43'51.7"N, 26 °17'14.0"E) and Staicele (Limbazu district 57°50'1.43"N, 24°44'27.43"E). Obtained samples were dried in an oven at 40 °C for 24 h, grinded and sieved through a 1 mm sieve. The fine fraction was then heated for 3 h at 950 °C to form calcium/iron composites.

2.2. Characterization methods of the adsorbents

Raw earth colour samples and obtained calcium/iron composites were characterised by X-ray powder diffraction (XRPD). The XRPD patterns were measured at ambient temperature using a D8 Advance powder diffractometer (Bruker, Germany), equipped with a LynxEye position-sensitive detector and Cu Kα radiation (λ = 1.54180 Å), 40 kV, 40 mA. Diffraction patterns were recorded with a 0.02 step size and a scan speed of 0.5 s per step from 5° to 65° of 2θ scale.

Differential scanning calorimetry/thermogravimetry (DSC/TGA) analysis was performed on TGA/DSC 2 thermogravimetric analyzer (Mettler Toledo, Switzerland). The samples were heated from 25 °C to 1050 °C at a rate of 10 °C per minute. Opened 70 μL aluminium oxide crucibles were filled with 10–15 mg of raw earth colour samples. A wide range of DSC/TG temperatures would provide the information for optimal conversional temperature to obtain calcium/iron composites from earth colour for phosphorus capture from wastewater.

The specific surface area (SSA) and pore size of the samples were determined by nitrogen adsorption-desorption isotherms at −196.15 °C (77.3 K) using a QUADRASORB SI (Quantachrome Corporation, USA) analyzer. Before the analysis, to remove excess moisture and impurities, the samples were outgassed under a vacuum at 300 °C for 3 h by Autosorb Degasser Model AD-9 (Anton Paar, England). The SSA was calculated by using the Brunauer-Emmett-Teller (BET) equation. The pore size and volume distribution were determined by the Density Functional Theory (DFT) model and micropore volume and pore size by the Dubinin-Radushkevich (DR) method. All calculations were performed by QuadraWinTM software that was supplied together with equipment.

Morphological characterization was done with a field emission scanning electron microscope (FE-SEM) Tescan MIRA\LMU (Czech Republic) using an accelerating voltage of 15 kV and a secondary electron detector (backscattered electron detector). The samples were attached to the SEM sample holder by a conductive carbon tape.

Scanning electron microscopy-energy dispersive X-ray analysis (SEM-EDX) was used for the identification of the chemical composition. EDX spectroscopic measurements were recorded with an Oxford Instruments X-Max 150 mm^2 silicon drift detector and analyzed using the INCA Energy Software. SEM-EDX analysis was done at an accelerating voltage of 15 kV. Calibration was done against the Ni standard.

2.3. Zeta potential and zero charge point

Initially, a suspension was made with 0,1 g of sample and 8 g of ultrapure water in individual vials. Samples were vortexed, and then the pH of the suspension was adjusted to 2, 4, 6, 8, 10, and 12 units using 1 M

hydrochloric acid (HCl) or 1 M sodium hydroxide (NaOH). To ensure hydration vials were placed on an orbital shaker for 30 min. After pH was tested and adjusted if necessary. All the samples were vortexed, and Zeta potential measurements were made using Zetasizer Nano ZS90 (Malvern Panalytical, United Kingdom).

2.4. Studies of phosphorus removal from artificial solution

A series of batch adsorption experiments were undertaken to evaluate the sorption capacity of the sorbents toward phosphorus, using a liquid-solid ratio of 2 g/L, consistent with the methodologies employed in similar studies by Delgadillo-Velasco et al. (2018) and Wu et al. (2021). Precisely 0.50 g of crushed into fine powder CaFeOxides and Polonite® were carefully transferred into individual 500 mL Erlenmeyer flasks. Subsequently, 250 mL of standard phosphate solution prepared from KH_2PO_4 was added (PO_4^{3-} concentrations ranged from 50 to 2000 mg/L) to composites. The obtained solid-liquid mixture was agitated at a rate of 160 rpm for 24 h at ambient temperature. The final supernatant was centrifugated at 2500 rpm for 10 min (LMC3000, Biosan). Quantification of remaining P was performed on spectrophotometer Hach 3900 coupled with the thermostat HT200S (Hach-Lange, Germany) by molybdovanadate method with acid persulfate digestion LCK 348. Before the analysis, samples were filtered through 0.45 μm syringe filters and diluted if necessary.

2.5. Sorption isotherms

The classic physical Langmuir (Langmuir, 1918) and empirical Freundlich (Freundlich, 1906) isotherm models were used to describe the sorption mechanism between the sorbate and the sorbent materials. The Langmuir isotherm suggests that sorption happens at homogenous sites on a sorbent's surface. Once a sorbate molecule occupies a site, that site cannot undergo further sorption. While the Freundlich isotherm describes sorption on heterogeneous surfaces. The analytical equations Eqs. (1) and (2) were as follows:

$$Langmuir: q_e = \frac{q_{max} \bullet K_L \bullet C_e}{1 + K_L \bullet C_e} \quad (1)$$

$$Freundlich: q_e = K_F \bullet C_e^{1/n} \quad (2)$$

where q_{max} (mg/g) is the theoretical monolayer capacity of the Langmuir equation, K_L (L/mg) is the Langmuir equilibrium constant, and C_e (mg/L) is the equilibrium solution concentration. K_F (L/mg) and n are Freundlich constants defining relative capacity and sorption intensity, respectively.

Additionally, Langmuir isotherm dimensionless constant, called the equilibrium parameter (R_L), was calculated with the following Eq. (3):

$$R_L = \frac{1}{1 + K_L \bullet C_0} \quad (3)$$

where C_0 is the highest initial sorbate concentration (mg/L) and the value of R_L indicates whether sorption will be favourable ($0 < R_L < 1$), unfavourable ($R_L > 1$), irreversible ($R_L = 0$), or linear ($R_L = 1$) (Weber and Chakravorti, 1974).

2.6. Studies of phosphorus removal from wastewater

Wastewater for jar tests was taken from the WWTP Daugavgriva (Latvia, Riga, 800,000 people equivalents) inlet after grit chambers. This point was selected because of the higher concentration of phosphorus (20–40 mg/L). The average wastewater characteristics were: pH 7.14 ± 0.16, electrical conductivity 1556 ± 338 μS/cm, UV light absorption at 254 nm 1.49 ± 0.44 cm^{-1}, UV light absorption at 410 nm 1.32 ± 1 cm^{-1}, turbidity 233 ± 113 NTU, total phosphorus concentration of 22.74 ± 10.29 mg/L, PO_4-P 4.73 ± 1.0 mg/L, total suspended solids (TSS) 650 ± 302 mg/L, chemical oxygen demand (COD) 866 ± 147 mg/L, biological oxygen demand (BOD5) 360 ± 41 mg/L. If not used the same day, wastewater was stored at room temperature (20 ± 2 °C) and used within 3 days ensuring proper mixing. In that case parameters were measured before the experiments. All data are presented as mean values ± standard deviations.

Jar Test PB-700 (Phipps & Bird, USA) was used for coagulation/sorption experiments. Each jar was filled with 1,5 L wastewater and added 0, 1, 2, 3, 5, and 10 g/L of CaFeOxide or Polonite®. The solid-liquid ratios for jar tests were selected according to a previous study by Karasa et al. (2023). The test setup was: 1 min rapid mixing (313 rpm), 30 min slow mixing (41 rpm), and 1 h sedimentation.

Total phosphorus was analyzed with colourimeter Hach DR890 (Hach-Lange, Germany) and standard Hach protocol No. 8190. Before the analysis, samples were filtered through 0.45 μm syringe filters and diluted, if necessary. All experiments were done in triplicates and average values were calculated unless mentioned otherwise.

The phosphorus removal rate from wastewater per gram of sorbent was calculated using Eqs. (4) and (5):

$$Removal\% = \frac{C_o - C_e}{C_o} \times 100 \quad (4)$$

$$Q_e = \frac{C_0 - C_e}{M} \times V \quad (5)$$

where C_0 is the initial concentration (mg/L) of phosphorus in the wastewater, C_e is phosphorus concentration in solution after adsorption, Q_e is phosphorus adsorbed per g of the sorbent (adsorption capacity), M is the mass (g) of the sorbent, V is the volume of the wastewater (L).

2.7. Study of phytotoxicity of spent sorbents

Spent sorbent materials' phytotoxic effect on the early phase of plant growth was examined using common wheat seeding growth tests. Seeds of wheat (*Triticum aestivum* L., spring wheat "SHARKI", Latvia) were soaked in 1 % potassium permanganate ($KMnO_4$) solution for 20 min and rinsed with distilled water, then they were germinated at room temperature for 2 days until the length of the coleoptile was around 2 mm.

Seedling growth tests were performed using a hydroponic system, following a procedure similar to that described by Abdel-Ghani et al. (2016) and Liu et al. (2017). 10 germinated seeds were evenly arranged on a filter paper strip (30 × 5 cm), then covered with a second strip and rolled up. The rolls were then placed in plant tissue containers, in which mineral material - CaFeOxide (T or S) or Polonite® - was added in different concentrations (0, 10, 100, 250, 500, 1000 g/L). Containers with five rolls of sprouts were placed under fluorescent lamps (1400 lm, 39 lm/W, Osram, Germany), at room temperature (24 °C) for a week. Afterwards, the length of the first and second leaves of *T. aestivum*, shoot fresh and dry weight of seedlings and the water content in the leaves were determined. R software and RStudio (Integrated Development Environment, IDE) were used for data analysis and graphical representation (Rstudio 2023.12.0 + 369, R 4.3.2.). Two-way ANOVA was conducted to assess the effects of mineral materials (Factor 1) and their concentrations (Factor 2) on the first leaf, second leaf, dry weight and water content. Post-hoc comparisons were performed using Tukey's HSD test at $p < 0.05$, and letter grouping was applied to indicate significant differences between means.

3. Results and discussion

3.1. Characterization of the adsorbents

3.1.1. X-ray powder diffraction data

The main components of Staicele earth colour were identified as limonite ($FeO(OH)\cdot nH_2O$) or goethite ($FeO(OH)$), calcite ($CaCO_3$), with

some traces of quartz (SiO_2), while Talicka was rich in calcite and goethite. Thermal treatment at 950 °C for 3 h resulted in composites labeled as CaFeOxide S (for Staicele earth colour) and CaFeOxide T (for Talicka sample). Obtained CaFeOxide S composite mostly consisted of the Brownmillerite group mineral - Srebrodolskite $Ca_2Fe_2O_5$, while CaFeOxide T was a mixture of several compounds: hematite (Fe_2O_3), harmunite $Ca(Fe_2O_4)$ and calcium oxide (CaO) (Fig. 1).

Remarkably, Srebrodolskite - $Ca_2Fe_2O_5$ (the main component of CaFeOxide S) can be synthesized cheaply in large volumes (Vanags et al., 2021) from chemical compounds Fe(NO3)3·9H2O and Ca(NO3)2·4H2O. We found that CaFeOxide S forms a "hydroxide" Ca3Fe2(OH)12 when hydrolysed which can be regenerated back to initial CaFeOxide at high temperatures (Karasa et al., 2023).

3.1.2. Chemical composition

The SEM - EDX results showed that both CaFeOxides compositions were similar - mostly calcium (Ca), iron (Fe), and oxygen (O) (Table 1). Interestingly, both contained small amounts of P and sulphur (S) - with such small concentrations data are not quantitative, but rather qualitative. Also, CaFeOxide T contained ytterbium (Yb) - a rare-earth metal. Before wastewater treatment, CaFeOxide T exhibited a highly heterogeneous and irregular macroscopic structure, significantly affecting elements' detection. This structural variability c large variations in the elemental percentages detected by SEM - EDX analysis (see * in Table 1). P, magnesium (Mg), and sodium (Na) were detected when Fe concentrations were high, while Yb and S appeared when Ca was the dominant element. It is likely that Ca compounds form a film covering underlying Fe compounds, as confirmed by chemical mapping (data not shown). Araújo et al. (2024) observed a similar formation of Fe and Ca hydroxide films, where washing led to a significant decrease in P adsorption, indicating that Ca and Fe influence the reduction of P removal. After wastewater treatment, CaFeOxide T exhibited more homogenous structure and small variations in elemental analysis.

Potassium (K) and chlorine (Cl) were not detected before in CaFeOxide S but appeared after wastewater treatment. Ca content decreased due to the release of CaO (that was also confirmed by pH increase during jar tests). Chemical transitions occur in CaFeOxide S after wastewater treatment. In accordance with XRPD the initial compound, Srebrodolskite $Ca_2Fe_2O_5$ (M = 271.84 g/mol and Fe = 41.1 %), transfers into calcium iron hydroxide $Ca_3Fe_2(OH)_{12}$ (M = 436.01 g/mol and Fe = 25.6 %). The Fe ratio between these compounds is 1.6, consistent with the SEM-EDX results shown in Table 1, where 37.73/23.07 = 1.6.

Polonite had a more homogeneous structure when compared to both CaFeOxides. Polonite® (derived from opoka rock - mostly silica and calcium carbonate that after heat treatment transforms to CaO) consisted mostly of silicon (Si), Ca, and O. Phosphorus appeared after treatment of wastewater. Fe content increased from 1.44 to 11.30 %, probably due to adsorption of iron on the surface. Ca content decreased due to the release of CaO (that was also confirmed by pH increase in the jar tests).

3.1.3. Thermal analysis

The thermal behaviour of the raw iron oxide pigments was evaluated by differential scanning calorimetry/thermogravimetry (DSC/TGA) analysis (Fig. 2). Talicka earth colour sample demonstrated several endothermic processes with significant mass losses. The first endothermic peak appeared below 100 °C indicating a loss of 7.2 % of physically adsorbed water (1 T). The second event occurred between 650 °C and 780 °C indicating decarboxylation of calcite (2 T), reaching a mass loss of around 22.2 %.

Sample of Staicele earth colour performed three endothermic processes, two demonstrate thermal conversions of iron compounds (e.g. 1S process in intervals from 240 °C to 280 °C and mass loss of 4.3 %, 2S process from 600 °C to 650 °C with mass loss of 7.8 %). These processes can be attributed to the dehydration of limonite and a formation of hydroxyl groups - a part of the goethite - resulting in the formation of a hematite (Longa-Avello et al., 2017). This process can be described by Eq. (6):

$$2FeOOH{\cdot}nH_2O \rightarrow Fe_2O_3 + (n+1)H_2O \quad (6)$$

The third process was identified as calcite decomposition (3S) withmass loss of 18.6 %.

3.1.4. Morphological characterization

The SEM images showed that the surface morphology of CaFeOxide S consisted of irregular, spheroid-shaped particles forming various-sized

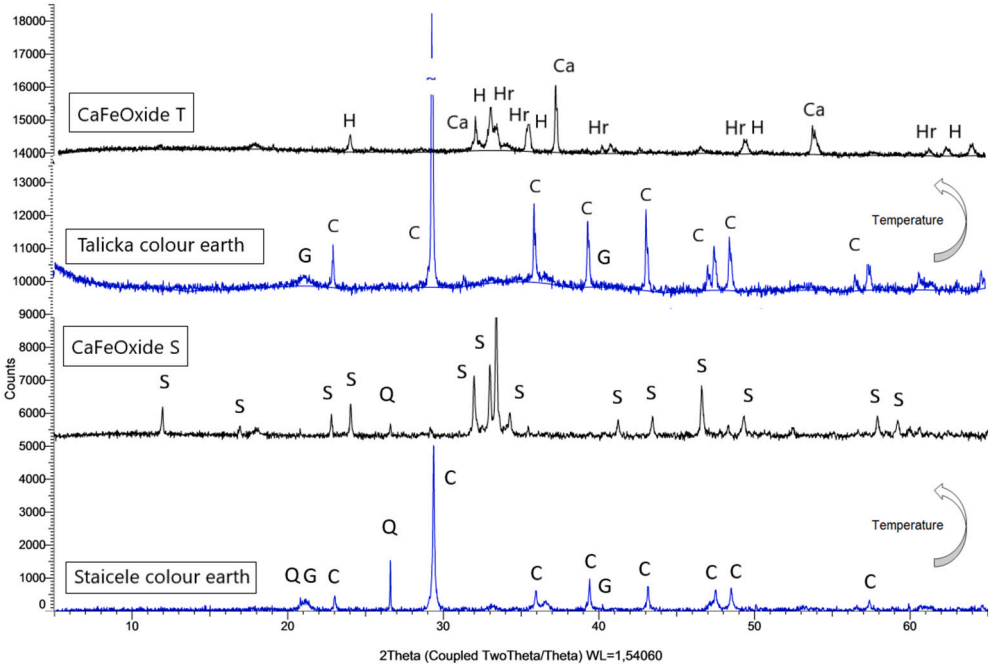

Fig. 1. PXRD patterns of raw materials and obtained Ca/FeOxides (C - calcite $CaCO_3$, G - iron oxide hydroxide, goethite, FeO(OH), Hr - harmunite $Ca_2(Fe_2O_4)$, S - Srebrodolskite Ca2Fe2O5, H - hematite Fe_2O_3, Ca - calcium oxide CaO, Q - quartz SiO2).

Table 1
Chemical composition of the adsorbents before and after treatment of wastewater, data obtained by SEM-EDX.

Sample	Element weight, %												
	O	Mg	Al	Si	P	S	Ca	Mn	Fe	Na	Yb	K	Cl
CaFeOxide S													
before	24.50	0.23	0.19	1.55	0.25	0.27	34.89	0.68	37.73				
after	44.57	0.44	1.65	3.31	0.21		27.38	6.84	23.07			0.88	0.63
CaFeOxide T													
before	38.09	0.19		1.75	0.83	0.07	33.02		17.75[a]	0.16	3.53		
after	44.67	0.78		2.80	0.70	0.18	23.27	0.25	26.62		0.89		0.26
Polonite®													
before	54.96	0.31	2.23	22.48			17.90		1.44			0.69	
after	51.29	0.66	1.63	21.57	0.56		11.98		11.30			0.54	

[a] The number represents an average result of 5 points. Two of them have Fe content below 1 %.

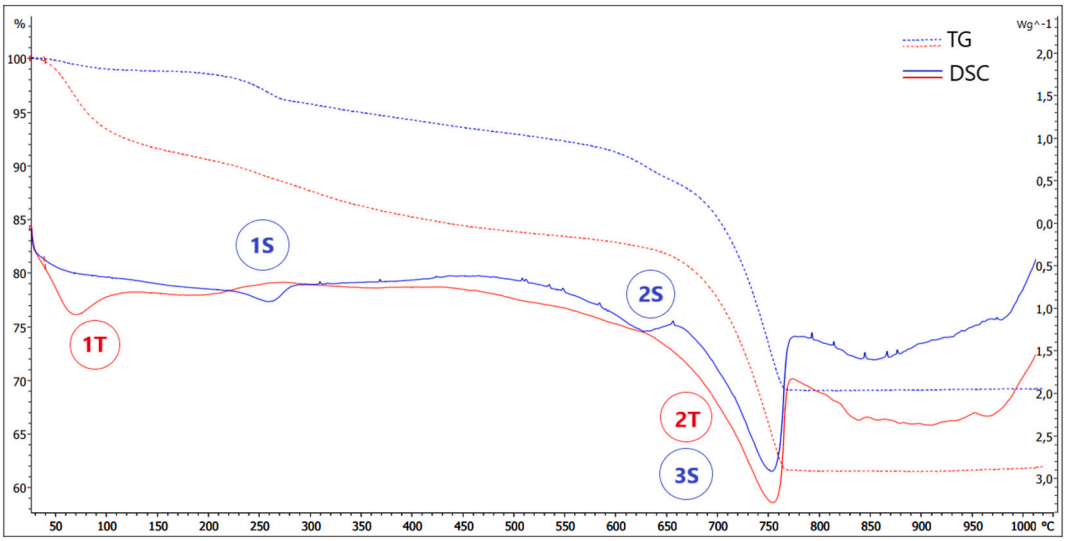

Fig. 2. DSC/TGA curves for raw earth colour samples from Talicka (1 T–2 T) and Staicele (1S—3S).

agglomerates (Fig. 3 a), similar to findings by Gupta et al. (2015), Bedon et al. (2021), and Karasa et al. (2023), characteristic of Brownmillerite group minerals.

After P adsorption, CaFeOxide S exhibited more spheroid-shaped particles (Fig. 3 d). CaFeOxide T had a sponge-like, porous structure with globular particles (Fig. 3 b), consistent with x-ray powder diffraction data and studies by Bloesser et al. (2020) and Gunawardhana et al. (2020), indicating hematite and harmunite minerals, while after P adsorption, a mixture of sheet-like particles appeared (Fig. 3 e). Polonite®, in contrast, consisted of wavy sheet-like particles (Fig. 3 c), as shown by Gubernat et al. (2023), and after P adsorption, it exhibited a flower-like structure consisting of nanosheets and fine-grained polycrystals (Fig. 3 f).

3.1.5. *Surface area and pore structure of adsorbents*

The specific surface area (SSA) increased in the order: CaFeOxide S < CaFeOxide T < Polonite® (Table 2). Polonite's® SSA was >6 times higher than that of the CaFeOxides samples. Additionally, Polonite® had significantly higher micropore (< 2 nm) and mesopore (2–40 nm) volumes, at 0.011 and 0.048 m^3/g, respectively, indicating a potentially higher sorption capacity toward P. While, CaFeOxide T had the largest micropores - 2.328 nm, which aligns with SEM data showing sponge-like particle morphology (Fig. 3).

3.2. *Phosphorus sorption studies*

3.2.1. *Adsorption isotherms*

Phosphorus sorption data for the developed Ca/FeOxides and commercially available sorbent Polonite® from phosphate aqueous solutions in controlled conditions is illustrated in Fig. 4. The Langmuir and Freundlich isotherm parameters from experimental data are shown in Table 2. The high correlation coefficient ($R^2 > 0.89$) indicates that the Langmuir model best describes the sorption behaviour of CaFeOxide S and CaFeOxide T, suggesting monolayer sorption where only a limited number of surface sites are sorbed. For Polonite®, both Langmuir and Freundlich isotherms fit, indicating more complex sorption involving monolayer and multilayer mechanisms.

The Langmuir model's R_L values (between 0 and 1) suggest favourable phosphorus sorption for all adsorbents. The maximum sorption capacity (q_{max}) increased in the order: Polonite® < CaFeOxide S < CaFeOxide T, with CaFeOxide T having the highest sorption capacity of 83.33 mg P/g. This may relate to the freely available form of calcium (CaO) in CaFeOxide T, despite similar amounts of it in both proposed composites, while calcium content in Polonite® is two times lower. In the Freundlich model, for Polonite® the n value is >1, indicating favourable sorption across all concentrations, driven by physical processes.

Similar P sorption behaviours were found in other Ca/Fe-rich adsorbents, like Ca/Fe composite (Wu et al., 2021), Ca/Fe-rich biochar (Yu

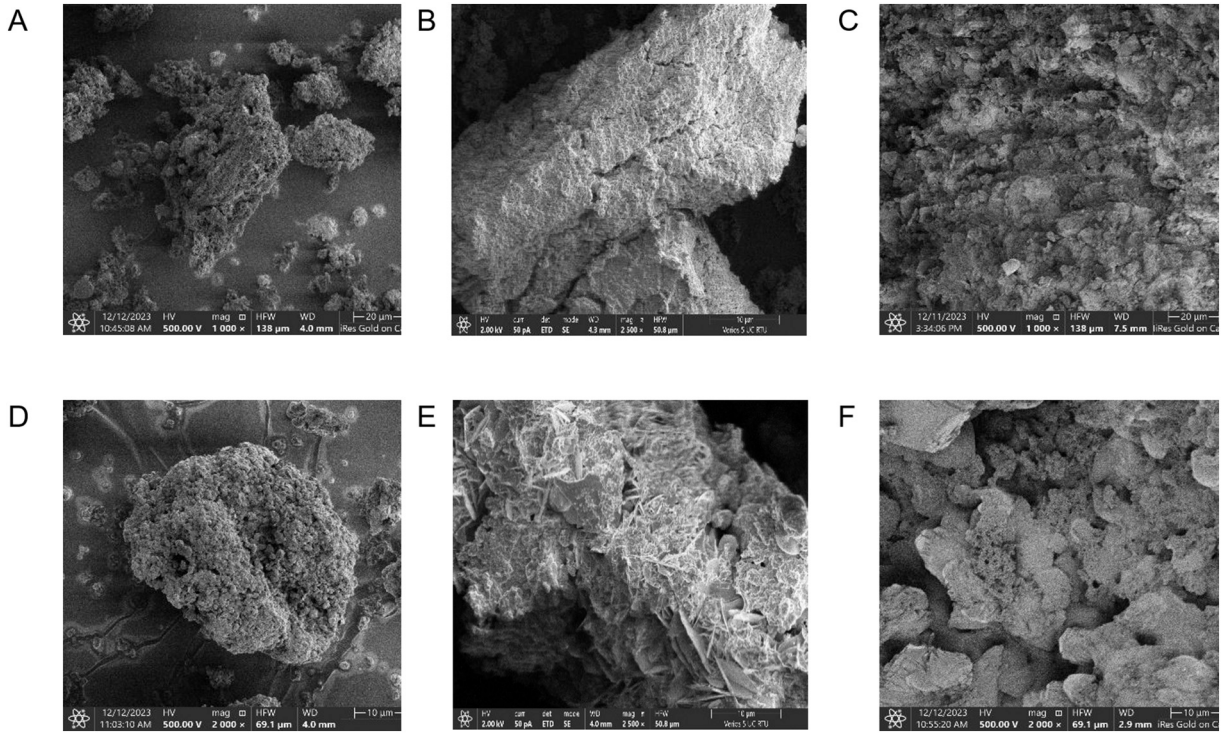

Fig. 3. SEM images (1 k, 2 k, 2,5 k magnification) of initial CaFeOxide S(a), CaFeOxide - T (b), Polonite® (c) and after P capture from wastewater CaFeOxide - S (d), CaFeOxide - T (e), Polonite® (f).

Table 2
Textural properties and Langmuir and Freundlich isotherm model parameters for the adsorption of phosphorus of studied adsorbents.

Sample	Parameter						
	Langmuir					*Freundlich*	
	q_{max} *(mg/g)*	K_L *(L/mg)*	R_L	R^2	*n*	K_F *(L/mg)*	R^2
CaFeOxide S	63.29	0.1763	0.0086	0.9977	3.19	15.4653	0.8436
CaFeOxide T	83.33	0.5634	0.0027	0.9960	3.68	38.3824	0.3914
Polonite®	53.19	0.0217	0.0661	0.9653	2.12	3.6226	0.9389
	Specific surface area, m^2/g	*Micropore volume,* m^3/g		*Micropore width, nm*	*Pore volume,* m^3/g		*Pore diameter, nm*
CaFeOxide S	2.588[a]	n/a		n/a	0.006*		4.678*
CaFeOxide T	4.149	0.002		2.328	0.015		4.152
Polonite®	24.148	0.011		1.588	0.048		4.152

[a] Data from Karasa et al. (2023).

et al., 2022), Fe oxide doped halloysite nanotubes (Almasri et al., 2019), Ca-rich sepiolite (Deng et al., 2021), which also fit the Langmuir model. We found that Polonite® maximum sorption capacity is 53.19 mg P/g, which aligns with literature demonstrating various sorption models: the Langmuir model with sorption capacities of 40.90 mg P/g (Karczmarczyk et al., 2017) and 36.26 mg P/g (Gubernat et al., 2023), and the Marczewski-Jaroniec model with sorption capacity of 54.33 mg P/g (Gubernat et al., 2023a). For other commercial sorbents like La-modified bentonite Phoslock® (10.1 mg P/g), Al-modified zeolite Aqual-P™ (29.9 mg P/g) and aluminium salts (251.1 mg P/g), the Langmuir model also is the best to describe mechanism for P sorption (Kang et al., 2022).

3.2.2. Phosphorus removal from wastewater

The results showed that all three tested adsorbents decreased P concentration in wastewater by at least 60 % (Fig. 5a). While the concentration of adsorbent increased from 1 to 10 g/L, the removal of phosphorus also increased from 37 % to 96 % for CaFeOxide S, from 38 % to 82 % for CaFeOxide T, and from 11 % to 60 % for Polonite®. The P adsorbed per g of sorbent decreases from 17.7 to 3.95 mg/g for CaFeOxide S, and from 11.63 to 4.96 mg/g for CaFeOxide T (Fig. 5b). A similar effect was observed by Lee et al. (2021) for calcium-rich waste materials. Polonite® exhibited a modest rise in P adsorption with higher adsorbent concentrations.

P removal by CaFeOxides involves several mechanisms, including physical adsorption, electrosorption, and precipitation, which occur simultaneously or complementarily. The authors suggest that precipitation, driven by calcium released from the composite's lime reacting with phosphate, plays a role. Traces of brushite ($CaHPO_4{\cdot}2H_2O$) were detected by XRPD after the batch experiments (data not shown), confirming the occurrence of precipitation. Similar studies have demonstrated that phosphate removal by Ca-rich sorbents primarily results from the formation of calcium-phosphate precipitates, such as brushite (Hermassi et al., 2017) or hydroxyapatite (Xu et al., 2023). While no distinct P-saturated crystalline phase was found in the solid residues after jar tests, the formation of a new phase between calcium and dissolved organic matter cannot be ruled out, as suggested by Yoon et al. (1998) and Chandrakanth and Amy (1998). It is also important to note

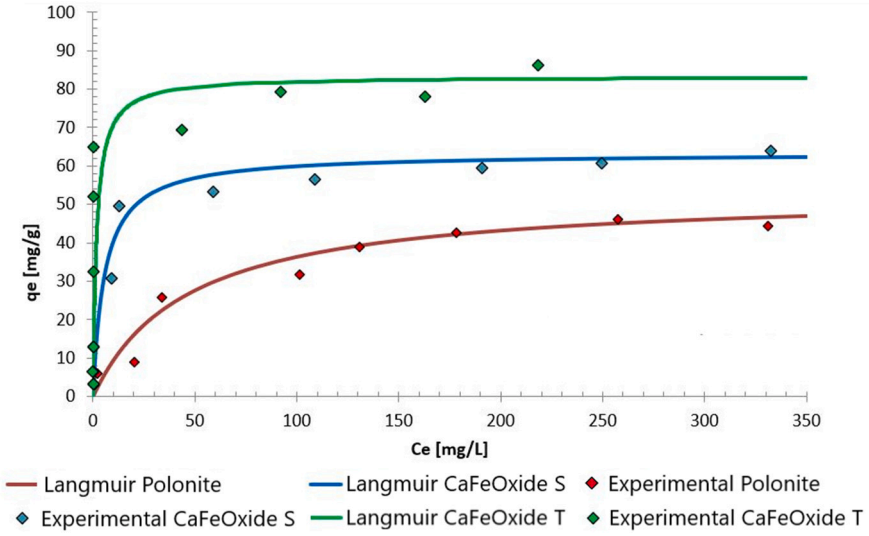

Fig. 4. Effect of initial concentration on the removal of phosphorus by studied adsorbents (experimental conditions: $m_{sorbent}$ = 0.50 g, Ci = 50–2000 mg/L PO_4^{3-}, contact time = 24 h, T = 24 °C).

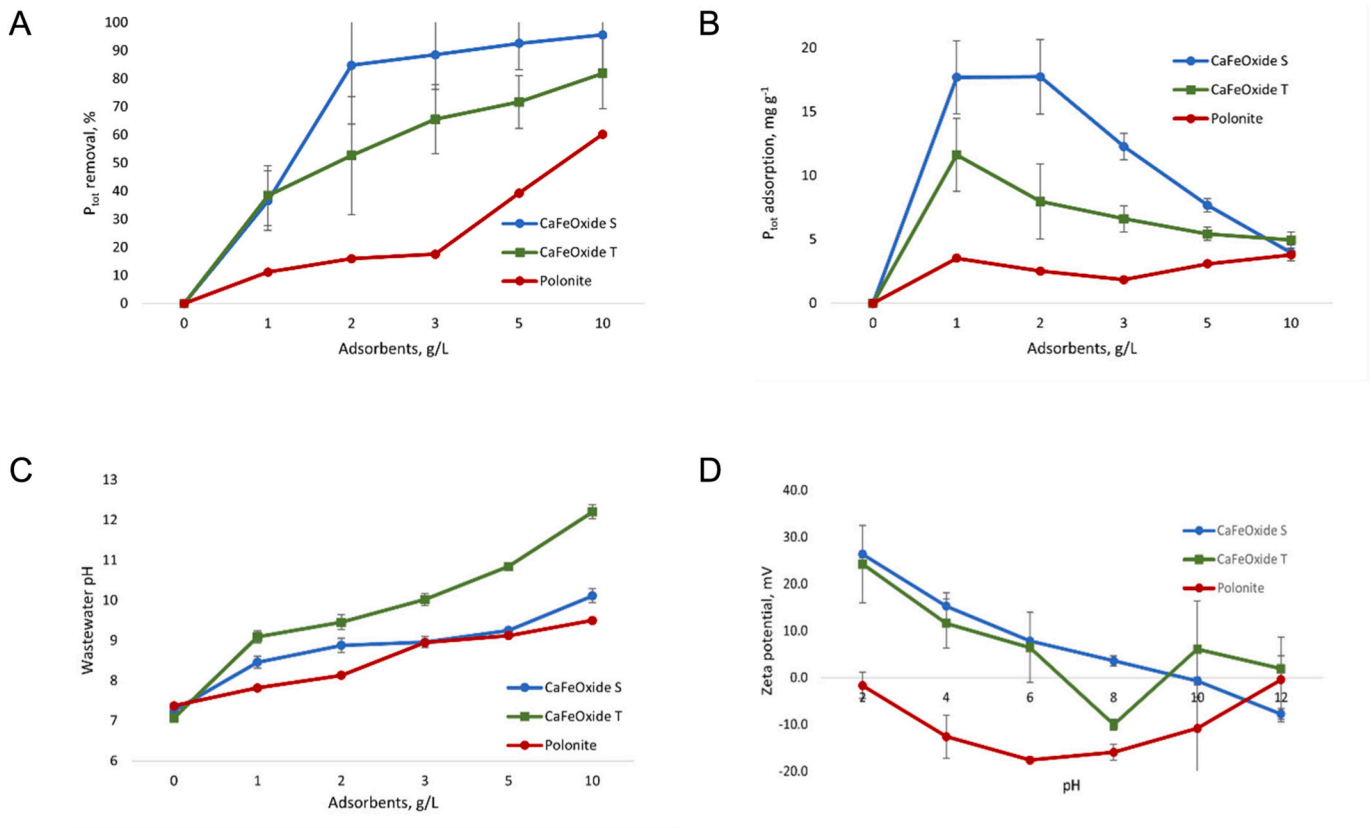

Fig. 5. (a) Phosphorus removal from wastewater versus adsorbent added, (b) P adsorbed per g of adsorbent versus adsorbent added (recalculated from decrease in a bulk), (c) changes in wastewater pH after addition of adsorbents, (d) Zeta potentials of adsorbents solutions as a function of pH.

that amorphous phases cannot be identified by XRPD.Despite this, P concentrations in the treated wastewater significantly decreased in the jar tests. This reduction, along with the Langmuir model, suggests that physical adsorption and electrostatic attraction between phosphates and Fe^{3+} ions are important mechanisms for P removal. These pathways are further supported by the increased solution pH and the SEM-EDX results.

3.2.3. *Effect of pH*

The form of phosphorus in a solution depends on the pH level. The predominant species are H_3PO_4 at approximately pH 2.15, $H_2PO_4^-$ between pH 2.15 and 7.20, HPO_4^{2-} from pH 7.20 to 12, and PO_4^{3-} at pH values above 12 (Liu et al., 2018). The pH of the wastewater used for sorption tests was 7.14 meaning that initially dominant P forms were $H_2PO_4^-$ and HPO_4^{2-}. But, after the addition of adsorbents pH increased up to 12.2 (Fig. 5c), changing dominant forms to HPO_4^{2-} and PO_4^{3-}. This is

because CaFeOxides release structural CaO in aqueous solutions leading to the formation of $Ca(OH)_2$ that increases pH.

The increase in pH caused by sorbent may be beneficial for reuse in amending acid soils, which are abundant in Latvia. An increase in pH also benefits heavy metals removal from wastewater (Gruškeviča et al., 2017; Comber et al., 2021). At pH levels below 8, phosphorus is removed primarily through physical adsorption. At pH levels above 8, the removal mechanism shifts to chemical precipitation (Lee et al., 1997; Kostura et al., 2017). This indicates that in the current study, the P removal occurred as adsorption for CaFeOxide S and Polonite, and as chemical precipitation for CaFeOxide T at doses above 3 g/L (Fig. 5c). In a previous study (Karasa et al., 2023) was tested if the removal is due to an increase of pH only. Results showed that the pH increase solely had a minor effect on P decrease.

Comparing the results of phosphorus adsorption in jar tests and adsorption capacity from artificial solutions (Section 3.2.1) - at the same ratio of sorbent to liquid 2 g/L. The results obtained with wastewater were approximately 4, 10 and 20 times lower for CaFeOxide S, CaFeOxide T, and Polonite®, respectively. This phenomenon may be explained by: the shorter time of experiment (1 h versus 24 h), the presence of competing ions and organics in wastewater (reducing available sites for phosphorus), and colloidal particles and particulate solids in wastewater (reducing surface area of sorbent). Other studies report P adsorption capacities for Polonite® of 1.5 mg/g (Cucarella et al., 2009) and 50 mg/kg (Renman and Renman, 2010) from real wastewater, whereas the results in this study indicate at least 2.5 times higher adsorption capacities.

3.2.4. Zeta potential and point of zero charge

The pH_{PZC} of CaFeOxide S was 10 (Fig. 5d), which indicates the best particle aggregation in an alkaline environment. For CaFeOxide T the graph dipped at pH 8. Polonite® showed two points of zero charge (around pH 2 and pH 12). However, all the results indicated that effective particle aggregation occurred at pH 4–12, as Zeta potential values were in the −20 to +20 mV range - which is considered favourable conditions for coagulation. In the jar tests with real wastewater Zeta potential values for all three sorbents stayed constant at −15 mV ± 1 regardless of sorbent dose.

3.3. Phytotoxic effect of P-loaded adsorbents

Obtained results showed that the addition of Polonite®, CaFeOxide S, and CaFeOxide T to the hydroponic system significantly increased overall vigour, first and second leaf length, water content and dry mass

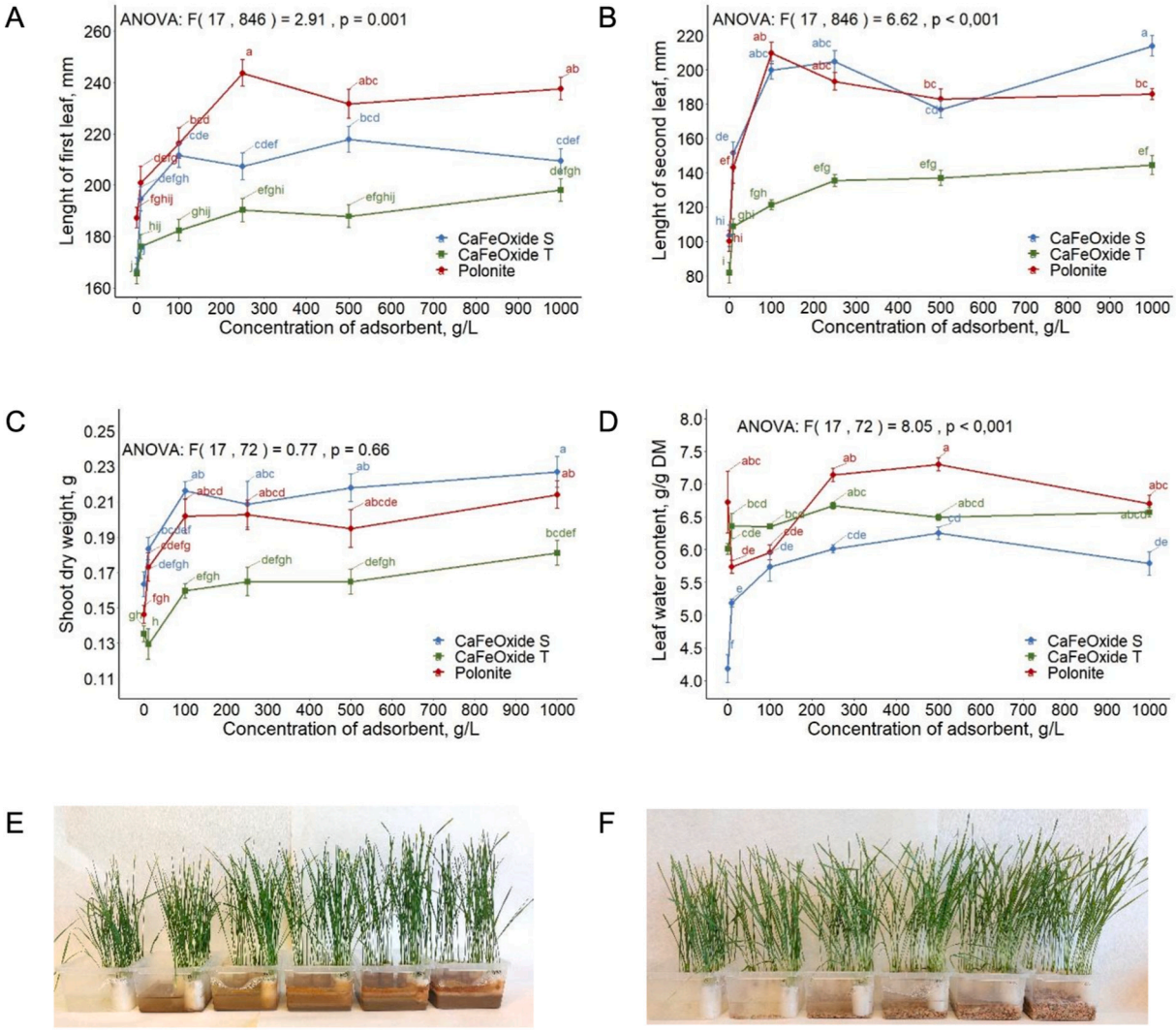

Fig. 6. Effect of different spent adsorbents on the first leaf (a), second leaf (b), on dry weight (c) and water content (d) of *T. aestivum* shoots; Images of *T. aestivum* growth in various concentrations of CaFeOxide S (e) and Polonite® (f) (from left to right: 0, 10, 100, 250, 500, 1000 g/L) after 7 days of the experiment. Different letters above the data points indicate statistically significant differences in ANOVA analysis ($p < 0.05$).

of shoots of *Triticum aestivum* with higher concentrations of spent adsorbents (Fig. 6). Ai et al. (2023) and Wang et al. (2020) also reported that adding P-loaded calcium-rich and iron-rich sorbents improved plant germination rates.

Polonite®, CaFeOxide S, and CaFeOxide T significantly increased *T. aestivum* first leaf growth at concentrations of 100, 10, and 250 g/L, respectively, resulting in leaf length increases of 29 mm, 29 mm, and 11 mm compared to the control. Plants achieved the greatest first leaf length of 216 mm at 100 g/L with Polonite® (Fig. 6 a). Also, the presence of spent adsorbents increased the second leaf length of *T. aestivum* (Fig. 6 b). For CaFeOxide S and Polonite® at 10 g/L concentration, the second leaf length was 48 mm and 43 mm, respectively, longer than the control sample. While CaFeOxide T reached the maximum length of the second leaf only at 100 g/L, and was 39 mm longer than the control sample. Additionally, the height of *T. aestivum* leaves that germinated during the entire experiment was chosen as the bioparameter for the calculation of the phytotoxicity index (Koval et al., 2023) by Eq. 7:

$$P = \frac{(B_c - B_i)}{B_c} \bullet 100\%, \quad (7)$$

where P is the phytotoxicity, %; B_c is the average first and second leaf height of the reference sample (distilled water), mm; B_i is the average first and second leaf height of the studied sample (spent adsorbent), mm.

In all cases, the phytotoxicity index was <20 % set as a limit value in Koval et al. (2023). For CaFeOxide S, CaFeOxide T and Polonite® depending on the used adsorbent concentration the phytotoxicity index ranged from −32 % to −66 %, from −20 % to −48 % and from −25 % to −56 %, respectively. Similarly, Koval et al. (2023) found that spent zeolite samples from wastewater treatment were non-toxic to winter barley germination.

The highest shoot dry mass was observed in seedlings grown with CaFeOxide S and Polonite®, showing an increase of 0.05 and 0.06 g, respectively at a concentration of 100 g/L. CaFeOxide T at 1000 g/L resulted in the lowest shoot dry mass (0.18 g). For all materials, shoot dry mass reached a plateau at 100 g/L (Fig. 6 c). CaFeOxides (T and S) increased *T. aestivum* seedlings' leaf water content (Fig. 6 d), resulting in an average of 6.14 g/g. Polonite®-treated plants had lower water content by 0.98 g/g at 10 g/L and 0.76 g/g at 100 g/L, compared to the control, but at 250 g/L, water content reached 7.14 g/g, surpassing CaFeOxides (T and S).

P is one of the plant nutrients that enhance seed germination and seedling growth (Yao et al., 2013). After phosphorus adsorption all tested adsorbents, significantly enhanced seedling growth parameters and the overall vigour of *T. aestivum*. However, further studies are needed to assess its effects on various plants and soils as well as understand P-loaded adsorbent long-term interactions with soil minerals. Also, other studies report that P-loaded Polonite® (Cucarella et al., 2009) and calcium/iron-rich adsorbents like Ca-loaded biochar (Ai et al., 2023), Fe-rich biochar (Wang et al., 2020), Fe-loaded pomegranate peel (Bellahsen et al., 2021), and iron-modified corn straw (Liu et al., 2015) enhance seed germination and plant growth, making them suitable as fertilizers and in Polonite® case also as soil amendment for liming.

4. Conclusions

In the present study P removal from municipal wastewater by mineral-based calcium/iron composites from Latvian iron oxide pigments was studied and spent sorbents phytotoxicity on plant growth was examined. The obtained data of CaFeOxides were compared to commercially available sorbent Polonite®. The obtained composites CaFeOxide S and CaFeOxide T demonstrated high phosphorus adsorption capacity (63.29 mg/g and 83.33 mg/g respectively) in artificial P solutions. Also, high P adsorption values were observed in real wastewater 11.63 and 17.7 mg P/g. Polonite® demonstrated the lowest values for artificial solutions and wastewater (53.19 mg/g and 2.51 mg/g respectively). The P removal mechanisms can be the simultaneous and/or complementary process of physical adsorption, electrosorption and precipitation.

Added spent sorbents to the hydroponic system significantly increased the overall vigour, leaf length, water content, and dry mass of *Triticum aestivum* shoots. Spent sorbents demonstrated no phytotoxic effects, showing potential for their suitability as fertilizers. However, further studies are needed to examine P-loaded CaFeOxides effects on various plants and soils as well as understand their long-term interactions with soil minerals. Additionally, the kinetics, thermodynamics and desorption of P are essential to fully evaluate the potential of the developed calcium/iron oxide composites for industrial sorbent production.

Funding

This research is funded by Fundamental and Applied Research project of the Latvian Council of Science "Unused Latvia's natural mineral resources for the development of innovative composite materials for phosphorus recovery from small municipal and industrial wastewater treatment plants to implement the principles of circular economy (CircleP, No. lzp-2021/1-0090)". The publication fee is covered by the TEN4 project "Allocation of state budget funding for tenure professorship to the Latvia University of Life Sciences and Technologies for 2024".

CRediT authorship contribution statement

Jūlija Karasa: Writing – original draft, Visualization, Methodology, Investigation, Data curation. **Rūta Ozola-Davidāne:** Writing – original draft, Project administration, Investigation, Conceptualization. **Kamila Gruškeviča:** Writing – original draft, Visualization, Investigation, Formal analysis. **Katrīna Anna Ozoliņa:** Writing – review & editing, Visualization. **Līga Irbe Mikosa:** Writing – review & editing, Resources. **Juris Kostjukovs:** Writing – review & editing, Validation, Supervision.

Declaration of competing interest

The authors declare that they have no known competing financial interests or personal relationships that could have appeared to influence the work reported in this paper.

Acknowledgement

Authors are greatly thankful to Diāna Mikanova who made the artwork for the graphical abstract.

Data availability

Data will be made available on request.

References

Abdel-Ghani, A.H., Sanchez, D.L., Kumar, B., Lubberstedt, T., 2016. Paper roll culture and assessment of maize root parameters. Bio-protocol 6 (18). https://doi.org/10.21769/bioprotoc.1926.

Ai, D., Ma, H., Meng, Y., Wei, T., Wang, B., 2023. Phosphorus recovery and reuse in water bodies with simple ball-milled Ca-loaded biochar. Sci. Total Environ. 860, 160502. https://doi.org/10.1016/j.scitotenv.2022.160502.

Almanassra, I., Kochkodan, V., Mckay, G., Atieh, M.A., Al-Ansari, T., 2021. Review of phosphate removal from water by carbonaceous sorbents. J. Environ. Manag. 287. https://doi.org/10.1016/j.jenvman.2021.112245.

Almasri, D.A., Saleh, N.B., Atieh, M.A., McKay, G., Ahzi, S., 2019. Adsorption of phosphate on iron oxide doped halloysite nanotubes. Sci. Rep. 9, 3232. https://doi.org/10.1038/s41598-019-39035-2.

Alshameri, A., Yan, C., Lei, X., 2014. Enhancement of phosphate removal from water by TiO2/Yemeni natural zeolite: preparation, characterization and thermodynamic. Microporous Mesoporous Mater. 196, 145–157. https://doi.org/10.1016/j.micromeso.2014.05.008.

Antunes, E., Jacob, M., Brodie, G., Schneider, P., 2018. Isotherms, kinetics and mechanism analysis of phosphorus recovery from aqueous solution by calcium-rich biochar produced from biosolids via microwave pyrolysis. J. Environ. Chem. Eng. 6 (1), 395–403. https://doi.org/10.1016/j.jece.2017.12.011.

Araújo, M.H.P., Ardisson, J.D., Krohling, A.C., Lago, R.M., Júnior, W.J., Tristão, J.C., 2024. Calcium ferrites for phosphate adsorption and recovery from wastewater. RSC Adv. 14 (3), 1612–1624. https://doi.org/10.1039/d3ra05871a.

Bacelo, H., Pintor, A., Santos, S., Boaventura, R., Botelho, C., 2020. Performance and prospects of different adsorbents for phosphorus uptake and recovery from water. Chem. Eng. J. 381, 122566. https://doi.org/10.1016/j.cej.2019.122566.

Barca, C., Magari, M., Miche, H., Hennebert, P., 2022. Effect of different wastewater composition on kinetics, capacities, and mechanisms of phosphorus sorption by carbonated bauxite residue. J. Environ. Chem. Eng. 10 (6), 108922. https://doi.org/10.1016/j.jece.2022.108922.

Battaz, S., Djazi, F., Allal, H., Trabelsi, I., Abdellah, Z., Benrabaa, R., Hamzaoui, A.H., 2024. Phosphorus recovery as struvite from wastewater by using seawater, brine and natural brine. Desalin. Water Treat. 317, 100082. https://doi.org/10.1016/j.dwt.2024.100082.

Bedon, A., Viricelle, J.P., Rieu, M., Mascotto, S., Glisenti, A., 2021. Single chamber solid oxide fuel cells selective electrodes: a real chance with brownmillerite-based nanocomposites. Int. J. Hydrog. Energy 46 (27), 14735–14747. https://doi.org/10.1016/j.ijhydene.2021.01.220.

Bellahsen, N., Kakuk, B., Beszédes, S., Bagi, Z., Halyag, N., Gyulavári, T., Kertész, S., Amarti, A.E., Tombácz, E., Hodúr, C., 2021. Iron-loaded pomegranate peel as a bio-adsorbent for phosphate removal. Water 13, 2709. https://doi.org/10.3390/w13192709.

Bloesser, A., Timm, J., Kurz, H., Milius, W., Hayama, S., Breu, J., Weber, B., Marschall, R., 2020. A novel synthesis yielding macroporous $CaFe_2O_4$ sponges for solar energy conversion. Sol. RRL 4 (8), 1900570. https://doi.org/10.1002/solr.201900570.

Chandrakanth, M.S., Amy, G.L., 1998. Effect of NOM source variations and calcium complexation capacity on ozone-induced particle destabilization. Water Res. 32 (1), 115–124. https://doi.org/10.1016/S0043-1354(97)00104-8.

Chen, Y.C., 2021. Phosphorus and nitrogen removal from water using steel slag in soil-based low-impact development systems. J. Water Process Eng. 44, 102385. https://doi.org/10.1016/j.jwpe.2021.102385.

Comber, S.D.W., Gardner, M.J., Ellor, B., 2021. Effects of iron dosing used for phosphorus removal at wastewater treatment works; impacts on forms of phosphorus discharged and secondary effects on concentrations and fate of other contaminants. Sci. Total Environ. 767, 145434. https://doi.org/10.1016/j.scitotenv.2021.145434.

Cucarella, V., Mazurek, R., Zaleski, T., Kopeć, M., Renman, G., 2009. Effect of Polonite used for phosphorus removal from wastewater on soil properties and fertility of a mountain meadow. Environ. Pollut. 157 (7), 2147–2152. https://doi.org/10.1016/j.envpol.2009.02.007.

Delgadillo-Velasco, L., Hernández-Montoya, V., Rangel-Vázquez, N.A., Cervantes, F.J., Montes-Morán, M.A., Moreno-Virgen, M., 2018. Screening of commercial sorbents for the removal of phosphates from water and modelling by molecular simulation. J. Mol. Liq. 262, 443–450. https://doi.org/10.1016/j.molliq.2018.04.100.

Deng, W., Zhang, D., Zheng, X., Ye, X., Niu, X., Lin, Z., Fu, M., Zhou, S., 2021. Adsorption recovery of phosphate from waste streams by Ca/Mg-biochar synthesis from marble waste, calcium-rich sepiolite and bagasse. J. Clean. Prod. 288, 125638. https://doi.org/10.1016/j.jclepro.2020.125638.

Faraji, B., Zarabi, M., Kolahchi, Z., 2020. Phosphorus removal from aqueous solution using modified walnut and almond wooden shell and recycling as soil amendment. Environ. Monit. Assess. 192 (6), 373. https://doi.org/10.1007/s10661-020-08326-x.

Feng, M., Li, M., Zhang, L., Luo, Y., Zhao, D., Yuan, M., Zhang, K., Wang, F., 2022. Oyster Shell modified tobacco straw biochar: efficient phosphate adsorption at wide range of pH values. Int. J. Environ. Res. Public Health 19, 7227. https://doi.org/10.3390/ijerph19127227.

Ferraro, A., de Sario, S., Attanasio, A., Di Capua, F., Gorgoglione, A., Fratino, U., Mascolo, M.C., Pirozzi, F., Trancone, G., Spasiano, D., 2023. Phosphorus recovery as struvite and hydroxyapatite from the liquid fraction of municipal sewage sludge with limited magnesium addition. J. Environ. Qual. 52, 584–595. https://doi.org/10.1002/jeq2.20446.

Freundlich, H.M.F., 1906. Over the adsorption in solution. J. Phys. Chem. 57, 385–471.

Gruškeviča, K., Būmanis, Ģ., Tihomirova, K., Bajāre, D., Juhna, T., 2017. Alkaline activated material as the adsorbent for uptake of high concentration of zinc from wastewater. Key Eng. Mater. Switzerland: Trans. Tech. Publ. 123-127. https://doi.org/10.4028/www.scientific.net/KEM.721.123.

Gubernat, S., Czarnota, J., Masłoń, A., Koszelnik, P., Pękala, A., Skwarczyńska-Wojsa, A., 2023. Efficiency of phosphorus removal and recovery from wastewater using marl and travertine and their thermally treated forms. J. Water Process Eng. 53, 103642. https://doi.org/10.1016/j.jwpe.2023.103642.

Gubernat, S., Masłoń, A., Czarnota, J., Koszelnik, P., Chutkowski, M., Tupaj, M., Gumieniak, J., Kramek, A., Galek, T., 2023a. Removal of phosphorus with the use of marl and travertine and their thermally modified forms—factors affecting the sorption capacity of materials and the kinetics of the sorption process. Materials 16, 1225. https://doi.org/10.3390/ma16031225.

Gunawardhana, B.P.N., Gunathilake, C.A., Dayananda, K.E.D.Y.T., Dissanayake, D.M.S.N., Mantilaka, M.M.M.G.P.G., Kalpage, C.S., Rathnayake, R.M.L.D., Rajapakse, R.M.G., Manchanda, A.S., Etampawala, T.N.B., Weerasekara, B.G.N.D., Fernando, P.N.K., Dassanayake, R.S., 2020. Synthesis of hematite nanodiscs from natural laterites and investigating their adsorption capability of removing Ni^{2+} and Cd^{2+} ions from aqueous solutions. J. Compos. Sci. 4, 57. https://doi.org/10.3390/jcs4020057.

Gupta, K., Singh, S., Rao, M.R., 2015. Fast, reversible CO2 capture in nanostructured Brownmillerite $CaFeO_2$. 5. Nano Energy 11, 146–153. https://doi.org/10.1016/j.nanoen.2014.10.016.

He, Y., Lin, H., Dong, Y., Liu, Q., Wang, L., 2016. Simultaneous removal of ammonium and phosphate by alkaline-activated and lanthanum-impregnated zeolite. Chemosphere 164, 387–395. https://doi.org/10.1016/j.chemosphere.2016.08.110.

Hermassi, M., Valderrama, C., Moreno, N., Font, O., Querol, X., Batis, N.H., Cortina, J.L., 2017. Fly ash as reactive sorbent for phosphate removal from treated waste water as a potential slow release fertilizer. J. Environ. Chem. Eng. 5 (1), 160–169. https://doi.org/10.1016/j.jece.2016.11.027.

Huang, W., Yu, X., Tang, J., Zhu, Y., Zhang, Y., Li, D., 2015. Enhanced adsorption of phosphate by flower-like mesoporous silica spheres loaded with lanthanum. Microporous Mesoporous Mater. 217, 225–232. https://doi.org/10.1016/j.micromeso.2015.06.031.

Jemeljanova, M., Ozola, R., Klavins, M., 2019. Physical-chemical properties and possible applications of clay minerals and humic acid composite materials. Agron. Res. 17 (S1), 1023–1032. https://doi.org/10.15159/ar.19.019.

Jing, X., Jiang, Y., Wang, Y., Liu, E., Cheng, R., Dai, J., Dai, X., Li, C., Yan, Y., 2020. Phosphate removal using free-standing functionalized mesoporous silica films with excellent recyclability. Microporous Mesoporous Mater. 296, 109953. https://doi.org/10.1016/j.micromeso.2019.109953.

Kang, L., Mucci, M., Lürling, M., 2022. Influence of temperature and pH on phosphate removal efficiency of different sorbents used in lake restoration. Sci. Total Environ. 812, 151489. https://doi.org/10.1016/j.scitotenv.2021.151489.

Karasa, J., Ozola-Davidane, R., Gruskevica, K., Mikosa, L.I., Kostjukovs, J., Kostjukova, S., Zekker, I., Krauklis, A., 2023. Use of calcium/iron oxide composites for sorption of phosphorus from wastewater. Agron. Res. 21 (3), 1161–1173. https://doi.org/10.15159/AR.23.055.

Karczmarczyk, A., Woja, K., Bliska, P., Baryła, A., Bus, A., 2017. The efficiency of filtration materials (Polonite® and Leca®) supporting phosphorus removal in on site treatment systems with wastewater infiltration. Infrastruktura i Ekologia Terenów Wiejskich (Infrastructure and Ecology of Rural Areas) 4, 1401–1413. https://doi.org/10.14597/infraeco.2017.4.1.107.

Kokins, A., Kostjukovs, J., Zarina, L., 2018. Natural iron oxide (earth colour) deposits in Latvia: an assessment of the possibilities for their use in inorganic pigment manufacturing. Color. Technol. 134. https://doi.org/10.1111/cote.12367.

Kostura, B., Dvorsky, R., Kukutschová, J., Študentová, S., Bednář, J., Mančík, P., 2017. Preparation of sorbent with a high active sorption surface based on blast furnace slag for phosphate removal from wastewater. Environ. Prot. Eng. https://doi.org/10.5277/epe170113.

Koval, M., Konohrai, V., Feshchenko, N., Romanenko, N., Yakymenko, I., 2023. Assessment of phytotoxicity of used zeolite as a sorbent of the dyeing and finishing production wastewater by the phytoindication method. Sci. Innov. 19 (6), 77–86. https://doi.org/10.15407/scine19.06.077.

Langmuir, I., 1918. The adsorption of gases on plane surfaces of glass, mica and platinum. J. Am. Chem. Soc. 40 (9), 1361–1403. https://doi.org/10.1021/ja02242a004.

Lee, S.H., Vigneswaran, S., Chung, Y., 1997. A detailed investigation of phosphorus removal in soil and slag media. Environ. Technol. 18 (7), 699–709. https://doi.org/10.1080/09593331808616588.

Lee, J., Oh, J., Yoo, S., Jho, E., Lee, C., Park, S., 2021. Removal of phosphorus from water using calcium-rich organic waste and its potential as a fertilizer for rice growth. J. Environ. Chem. Eng. 10 (2). https://doi.org/10.1016/j.jece.2022.107367.

Li, B., Boiarkina, I., Yu, W., Huang, H.M., Munir, T., Wang, G.Q., Young, B.R., 2019. Phosphorous recovery through struvite crystallization: challenges for future design. Sci. Total Environ. 648, 1244–1256. https://doi.org/10.1016/j.scitotenv.2018.07.166.

Li, X., Xu, Y., Shen, S., Guo, T., Dai, H., Lu, X., 2022. Effects of dissolved organic matter on phosphorus recovery via hydroxyapatite crystallization: new insights based on induction time. Sci. Total Environ. 822, 153618. https://doi.org/10.1016/j.scitotenv.2022.153618.

Li, B., Ng, S.J., Han, J.C., Li, M., Zeng, J., Guo, D., Zhou, Y., He, Z., Wu, X., Huang, Y., 2023a. Network evolution and risk assessment of the global phosphorus trade. Sci. Total Environ. 860, 160433. https://doi.org/10.1016/j.scitotenv.2022.160433.

Li, L., Zhu, Z., Ni, J., Zuo, X., 2023b. Sustainable phosphorus adsorption and recovery from aqueous solution by a novel recyclable Ca-PAC-CTS. Sci. Total Environ. 897, 165444. https://doi.org/10.1016/j.scitotenv.2023.165444.

Liu, F., Zuo, J., Chi, T., et al., 2015. Removing phosphorus from aqueous solutions by using iron-modified corn straw biochar. Front. Environ. Sci. Eng. 9, 1066–1075. https://doi.org/10.1007/s11783-015-0769-y.

Liu, Z., Gao, K., Shan, S., Gu, R., Wang, Z., Craft, E.J., Mi, G., Yuan, L., Chen, F., 2017. Comparative analysis of root traits and the associated QTLs for maize seedlings grown in paper roll, hydroponics and vermiculite culture system. Front. Plant Sci. 8 (436). https://doi.org/10.3389/fpls.2017.00436.

Liu, R., Chi, L., Wang, X., Sui, Y., Wang, Y., Arandiyan, H., 2018. Review of metal (hydr) oxide and other adsorptive materials for phosphate removal from water. J. Environ. Chem. Eng. 6 (4), 5269–5286. https://doi.org/10.1016/j.jece.2018.08.008.

Longa-Avello, L., Pereyra-Zerpa, C., Casal-Ramos, J.A., Delvasto, P., 2017. Study of the calcination process of two limonitic iron ores between 250 °C and 950 °C. Revista Facultad De Ingeniería 26 (45), 33–45. https://doi.org/10.19053/01211129.v26.n45.2017.6053.

Othman, A., Dumitrescu, E., Andreescu, D., Andreescu, S., 2018. Nanoporous sorbents for the removal and recovery of phosphorus from eutrophic waters: sustainability challenges and solutions. ACS Sustain. Chem. Eng. 6 (10), 12542–12561. https://doi.org/10.1021/acssuschemeng.8b01809.

Park, J.H., Wang, J.J., Seo, D.C., 2021. Sorption characteristics of phosphate by bauxite residue in aqueous solution. Colloids Surf. A Physicochem. Eng. Asp. 618, 126465. https://doi.org/10.1016/j.colsurfa.2021.126465.

Park, J., Choi, A., Lee, S., Lee, J.H., Rho, J.S., Kim, S.H., Seo, D.C., 2022. Removal of phosphates using eggshells and calcined eggshells in high phosphate solutions. Appl. Biol. Chem. 65, 75. https://doi.org/10.1186/s13765-022-00744-4.

Ping, Q., Zhang, Z., Guo, W., Wang, L., Li, Y., 2024. A comprehensive investigation to the fate of phosphorus in full-scale wastewater treatment plants using aluminum salts for enhanced phosphorus removal. Sci. Total Environ. 913, 169641. https://doi.org/10.1016/j.scitotenv.2023.169641.

Renman, A., Renman, G., 2010. Long-term phosphate removal by the calcium-silicate material Polonite in wastewater filtration systems. Chemosphere 79 (6), 659–664. https://doi.org/10.1016/j.chemosphere.2010.02.035.

Saaremäe, E., Liira, M., Poolakese, M., Tamm, T., 2014. Removing phosphorus with Ca-Fe oxide granules - a possible wetlands filter material. Hydrol. Res. 45, 368. https://doi.org/10.2166/nh.2013.101.

Salimova, A., Zuo, J., Liu, F., Wang, Y., Wang, S., Verichev, K., 2020. Ammonia and phosphorus removal from agricultural runoff using cash crop waste-derived biochars. Front. Environ. Sci. Eng. 14, 48. https://doi.org/10.1007/s11783-020-1225-1.

Spears, B.M., Brownlie, W.J., Cordell, D., Hermann, L., Mogollón, J.M., 2022. Concerns about global phosphorus demand for lithium-iron-phosphate batteries in the light electric vehicle sector. Commun. Mater. 3, 14. https://doi.org/10.1038/s43246-022-00236-4.

Szota, C., Danger, A., Poelsma, P.J., Hatt, B.E., James, R.B., Rickard, A., Burns, M.J., Cherqui, F., Grey, V., Coleman, R.A., Fletcher, T.D., Fletcher, T.D., 2024. Developing simple indicators of nitrogen and phosphorus removal in constructed stormwater wetlands. Sci. Total Environ. 928, 172192. https://doi.org/10.1016/j.scitotenv.2024.172192.

Vanags, M., Mežule, L., Spule, A., Kostjukovs, J., Šmits, K., Tamm, A., Juhna, T., Vihodceva, S., Käämbre, T., Baumane, L., Začs, D., Vasiliev, G., Turks, M., Mierina, I., Sherre, P.C., Šutka, A., 2021. Rapid catalytic water disinfection from earth abundant $Ca_2Fe_2O_5$ Brownmillerite. Adv. Sustain. Syst. https://doi.org/10.1002/adsu.202100130.

Vu, M.T., Duong, H.C., Wang, Q., Cai, Z., Hoang, N.B., Thi, Viet N., T., Nghiem L. D., 2023. A low-cost method using steel-making slag to quench the residual phosphorus from wastewater effluent. Environ. Technol. Innov. 31, 103181. https://doi.org/10.1016/j.eti.2023.103181.

Wang, H., Xiao, K., Yang, J., Yu, Z., Yu, W., Xu, Q., Liang, S., Hu, J., Hou, H., Liu, B., 2020. Phosphorus recovery from the liquid phase of anaerobic digestate using biochar derived from iron−rich sludge: a potential phosphorus fertilizer. Water Res. 174, 115629. https://doi.org/10.1016/j.watres.2020.115629.

Wang, Q., Liao, Z., Yao, D., Yang, Z., Wu, Y., Tang, C., 2021. Phosphorus immobilization in water and sediment using iron-based materials: a review. Sci. Total Environ. 767, 144246. https://doi.org/10.1016/j.scitotenv.2020.144246.

Wang, S., Li, N., Yuan, Q., Liang, D., Chang, J., Wang, X., Ren, N., 2023. Vivianite recovery from high concentration phosphorus wastewater with mine drainage as iron sources. Sci. Total Environ. 858, 160098. https://doi.org/10.1016/j.scitotenv.2022.160098.

Weber, T.W., Chakravorti, R.K., 1974. Pore and solid diffusion models for fixed-bed adsorbers. Am. Inst. Chem. Eng. J. 20 (2), 228–238. https://doi.org/10.1002/aic.690200204.

Wu, D., Tian, S., Long, J., Peng, S., Xu, L., Sun, W., Chu, H., 2021. Remarkable phosphate recovery from wastewater by a novel Ca/Fe composite: synergistic effects of crystal structure and abundant oxygen-vacancies. Chemosphere 266, 129102. https://doi.org/10.1016/j.chemosphere.2020.129102.

Xu, C., Liu, R., Tang, Q., Hou, Y., Chen, L., Wang, Q., 2023. Adsorption removal of phosphate from rural domestic sewage by Ca-modified biochar derived from waste eggshell and sawdust. Water 15 (17), 3087. https://doi.org/10.3390/w15173087.

Yao, Y., Gao, B., Chen, J., Yang, L., 2013. Engineered biochar reclaiming phosphate from aqueous solutions: mechanisms and potential application as a slow-release fertilizer. Environ. Sci. Technol. 47 (15), 8700–8708. https://doi.org/10.1021/es4012977.

Yin, Q., Liu, M., Ren, H., 2019. Biochar produced from the co-pyrolysis of sewage sludge and walnut shell for ammonium and phosphate adsorption from water. J. Environ. Manag. 249. https://doi.org/10.1016/j.jenvman.2019.109410.

Yoon, S.H., Lee, C.H., Kim, K.J., Fane, A.G., 1998. Effects of calcium ion on the fouling of nanofilter by humic acid in drinking water production. Water Res. 32 (7), 2180–2186. https://doi.org/10.1016/S0043-1354(97)00416-8.

Yu, J., Li, X., Wu, M., Lin, K., Xu, L., Zeng, T., Shi., H., Zhang, M., 2022. Synergistic role of inherent calcium and iron minerals in paper mill sludge biochar for phosphate adsorption. Sci. Total Environ. 834, 155193. https://doi.org/10.1016/j.scitotenv.2022.155193.